The American Journal of Human Genetics, Volume *107*

Supplemental Data

High-Throughput Reclassification of *SCN5A* Variants

Andrew M. Glazer, Yuko Wada, Bian Li, Ayesha Muhammad, Olivia R. Kalash, Matthew J. O'Neill, Tiffany Shields, Lynn Hall, Laura Short, Marcia A. Blair, Brett M. Kroncke, John A. Capra, and Dan M. Roden

Table of Contents

Figure S1. Diagram of cloning and cell line generation

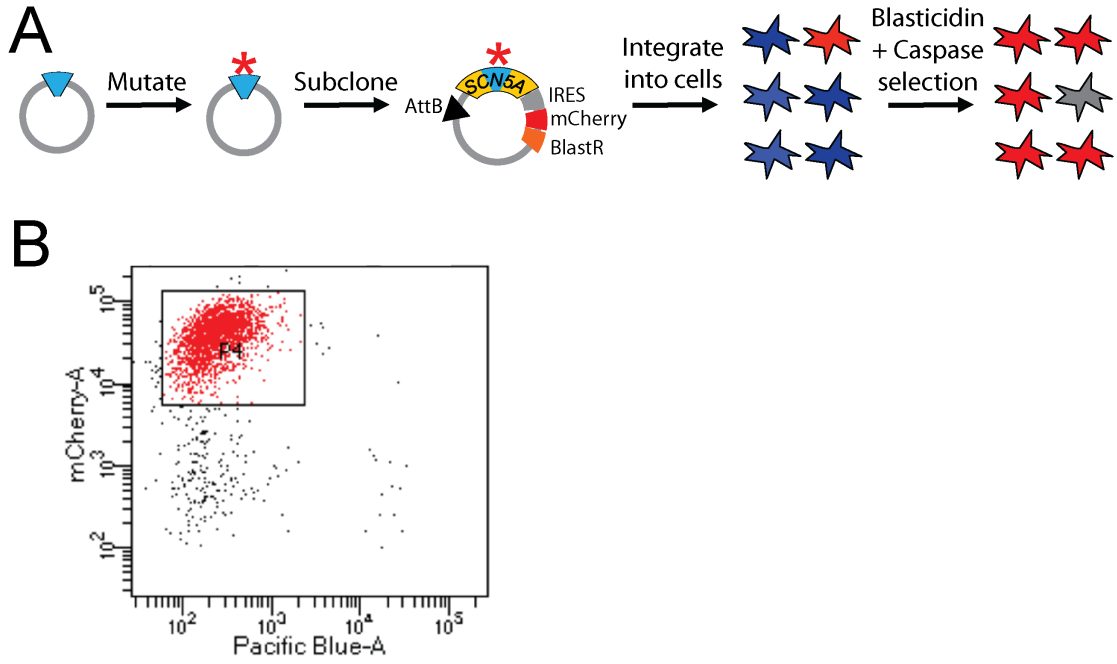

Figure S2. Voltage protocols used in this study

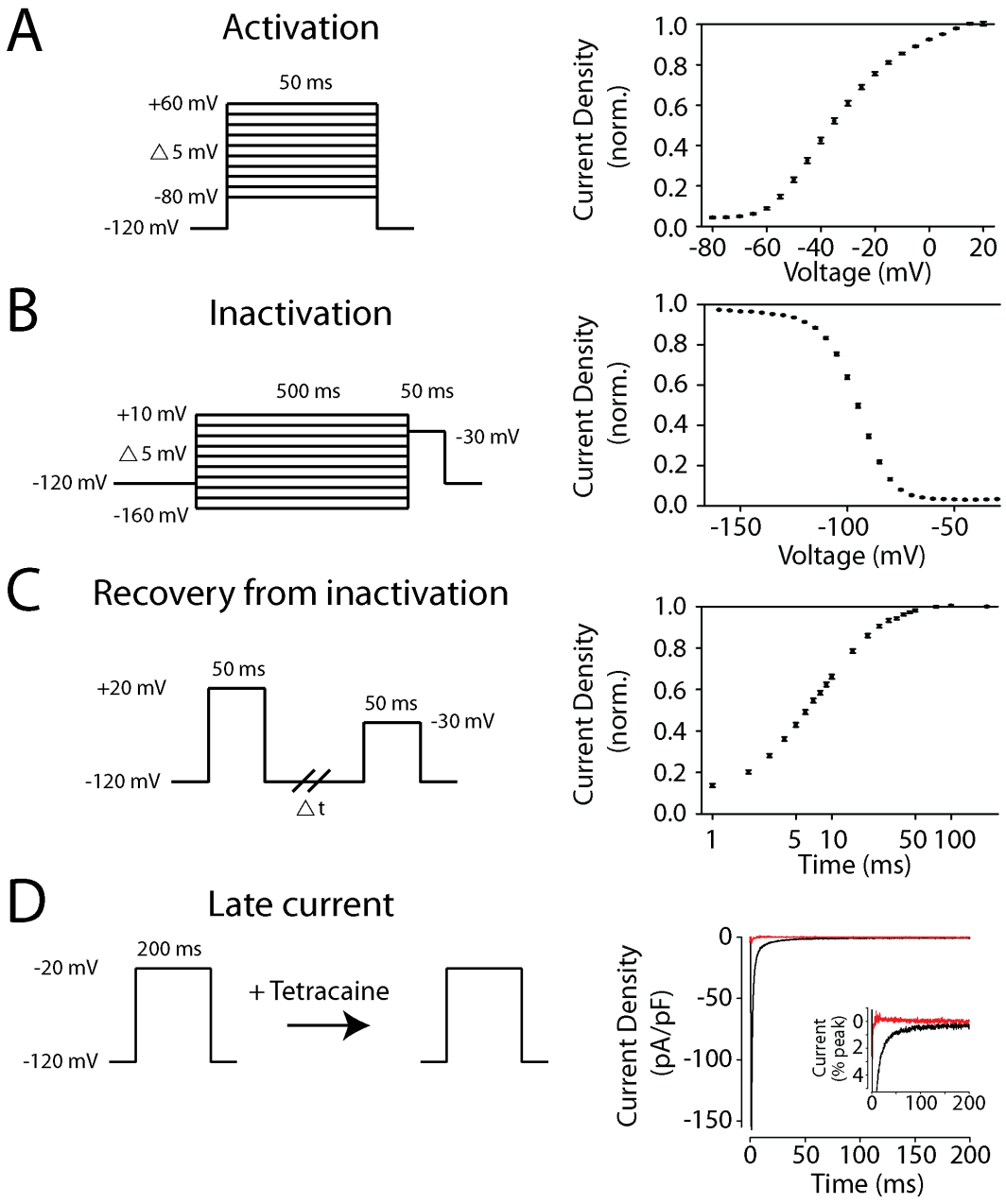

Figure S3. Example sodium current traces from included and excluded wells

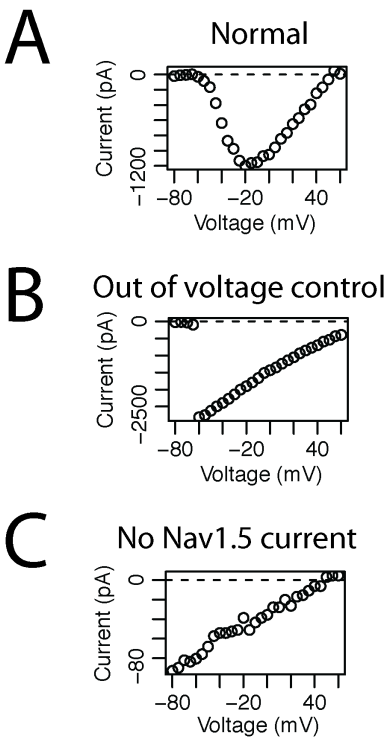

A) Example well with $Na_V1.5$ current that would be included in the analysis. B) Example well with $Na_V1.5$ current that is out of voltage control. This well would be excluded from the analysis. C) Example well with no substantial $Na_V1.5$ current. Note the difference in y-axis scale between panels.

Figure S4: Classification criteria

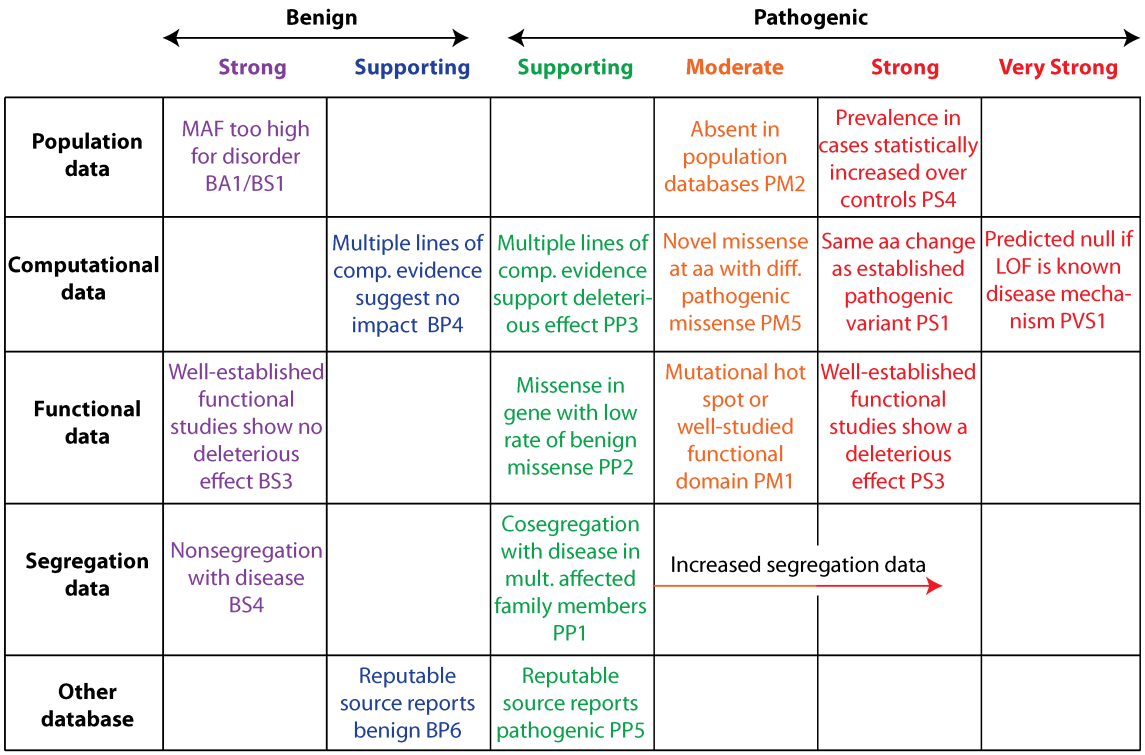

Diagram of American College of Medical Genetics and Genomics classification criteria, with a focus on criteria relevant for classification of *SCN5A* missense variants. Figure is adapted from Richards et al, 2015.[1]

Figure S5. A structural model of human $Na_V1.5$

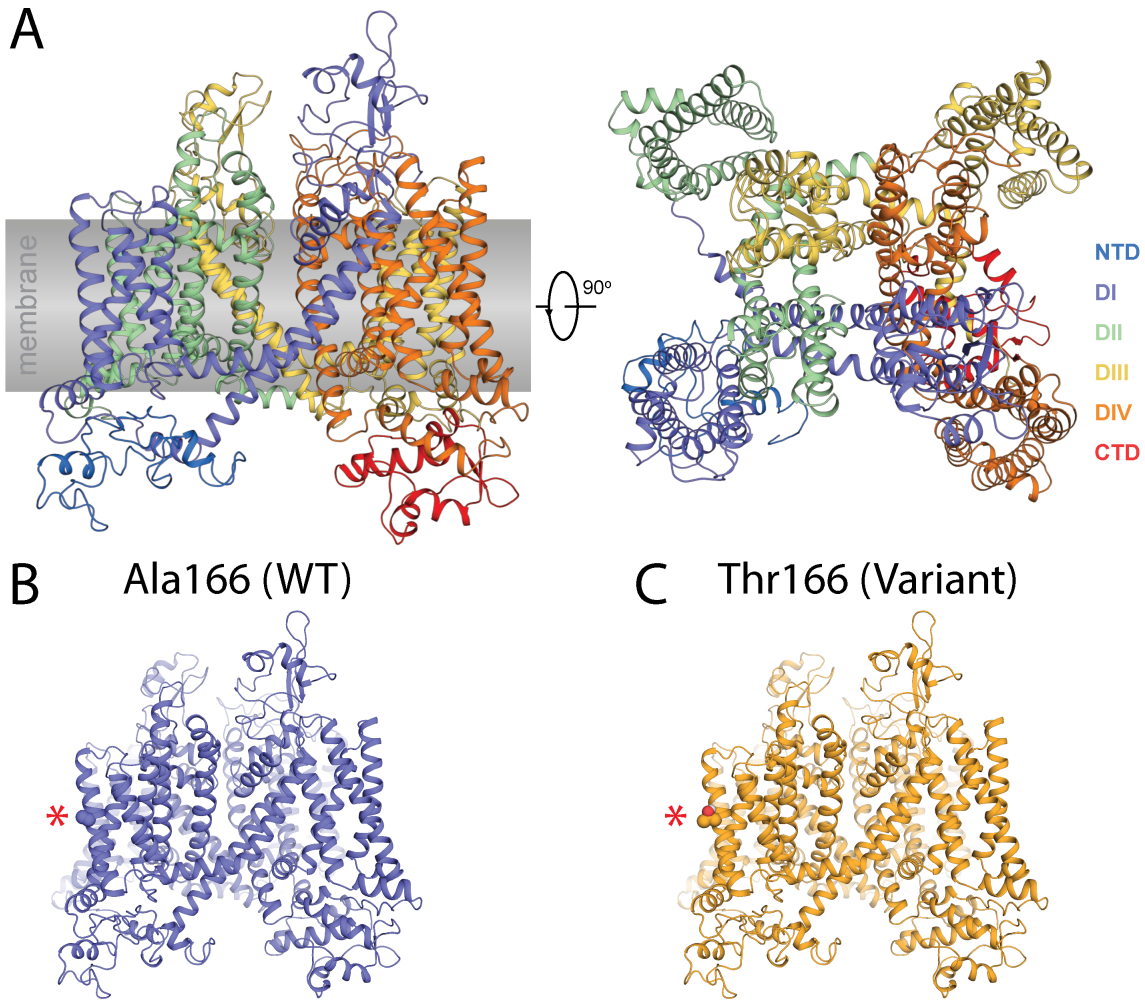

A) Wildtype $Na_V1.5$ model. The N-terminal domain (NTD), four homologous ion channel domains (DI through DIV) each consisting of six transmembrane helices, and C-terminal domain (CTD) are color-coded. B-C) A suspected benign variant, p.Ala166Thr, has a low predicted impact on protein structure and wild-type-like electrophysiological properties.

Figure S6: Voltage dependence of activation

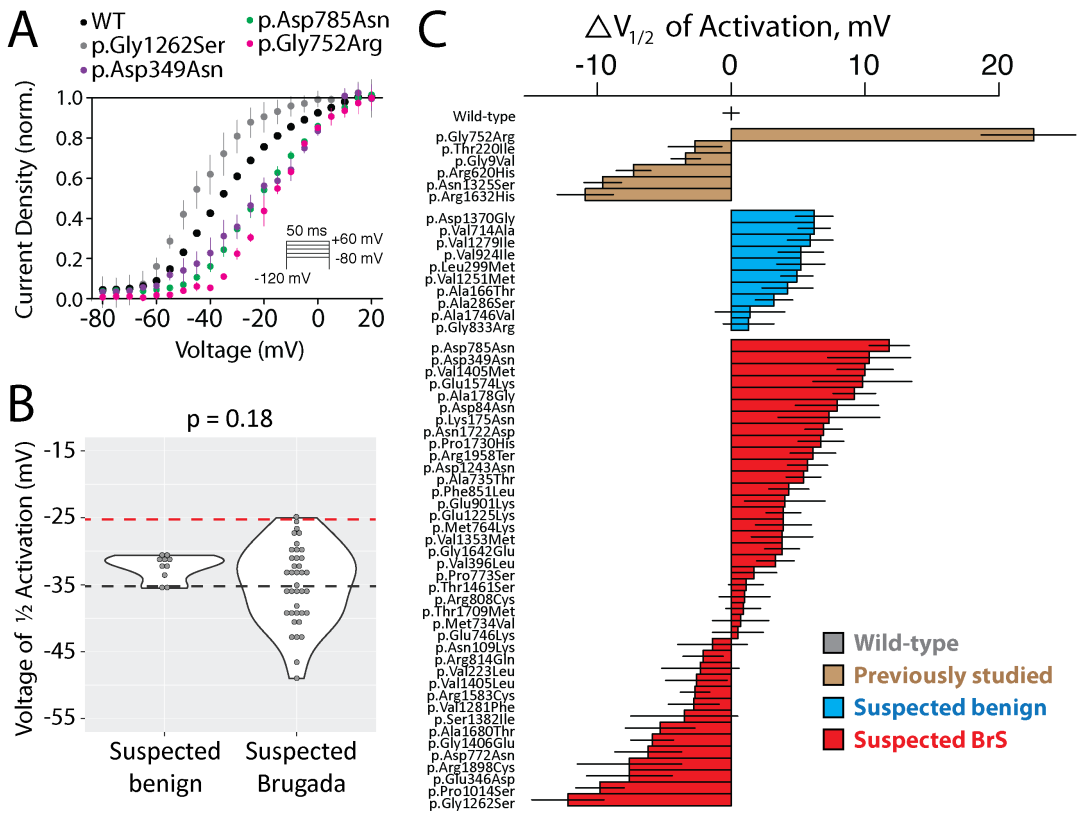

A) Normalized activation curves for wild-type, p.Asp785Asn and p.Asp349Asn (the two suspected BrS-associated variants with >10 mV rightward shifts in $V_{1/2}$ activation), p.Gly1262Ser (a suspected Brs-associated variant with a leftward shift) and p.Gly752Arg, a previously studied variant with a large rightward shift, as has previously been observed.[2] All of these variants also have a reduction in peak current (Figure 2). Error bars indicate standard error of the mean. B) Violin plot of $V_{1/2}$ activation. Black line indicates wild-type value and red line indicates a 10 mV shift in activation. Two variants, p.Asp785Asn and p.Asp349Asn, have >10 mV rightward shift in activation voltage. Panel same as Figure 2E. C) Barplot of wild-type (grey), previously studied (brown), suspected benign (blue), or suspected Brugada Syndrome-associated voltage of ½ activation. Bars indicate mean +/- standard errors. Only variants with

at least 5 qualifying cells were included, so most severe loss of function variants are not included.

Figure S7: Inactivation time

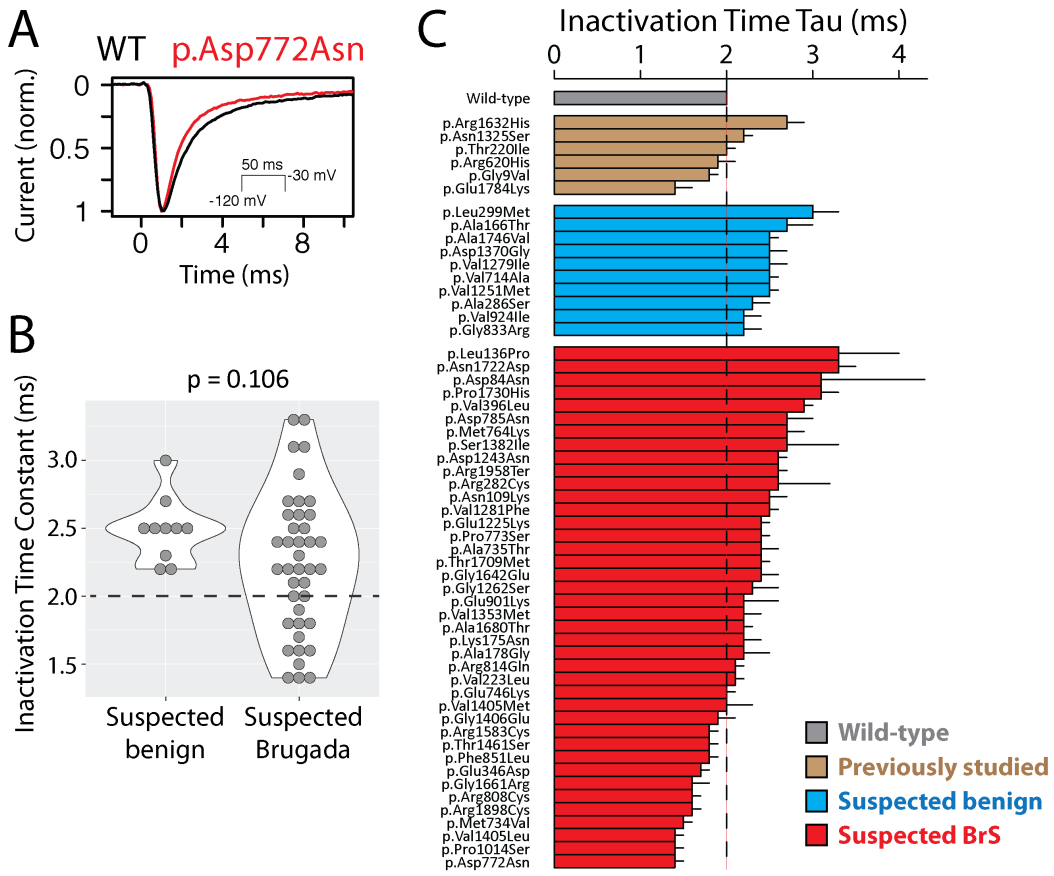

A) Inactivation time for wild-type and the suspected Brugada Syndrome-associated variant with the shortest time constant of inactivation, p.Asp772Asn. Inactivation time was measured from a 50ms pulse from -120 mV to -30 mV. Representative traces that had inactivation time constants closest to the mean values were selected. B) Violin plot of inactivation time constant. Black line indicates wild-type value. C) Barplot of wild-type (grey), previously studied (brown), suspected benign (blue), or suspected Brugada Syndrome-associated inactivation time. Bars indicate mean +/- standard errors. Only variants with at least 5 qualifying cells were included, so most severe loss of function variants are not included.

Figure S8: Voltage dependence of inactivation

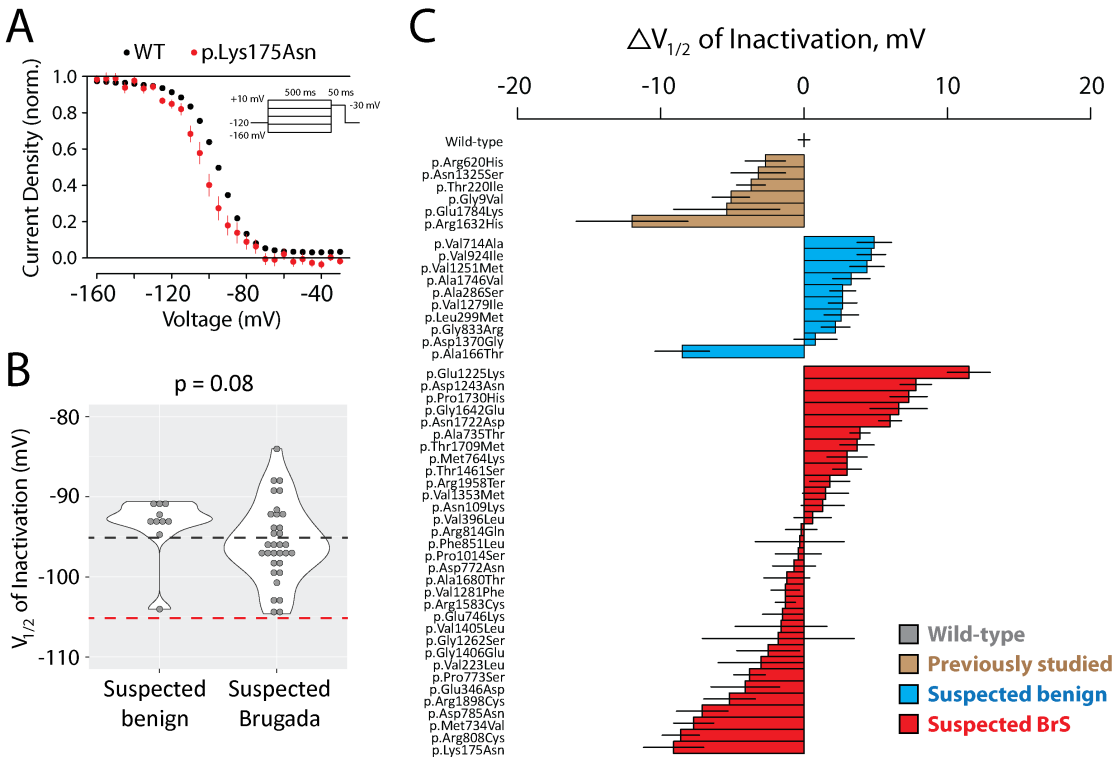

A) Normalized inactivation curves for wild-type and p.Lys175Asn, a suspected Brugada syndrome-associated variant that has the largest observed leftward shift in $V_{1/2}$ inactivation. Error bars indicate standard error of the mean. B) Violin plot of $V_{1/2}$ inactivation. Black line indicates wild-type value and red line indicates a 10 mV shift in inactivation. No previously unstudied variants had a >10 mV leftward shift in inactivation voltage. C) Barplot of wild-type (grey), previously studied (brown), suspected benign (blue), or suspected Brugada Syndrome-associated voltage of ½ inactivation. Bars indicate mean +/- standard errors. Only variants with at least 5 qualifying cells were included, so most severe loss of function variants are not included.

Figure S9: Recovery from inactivation

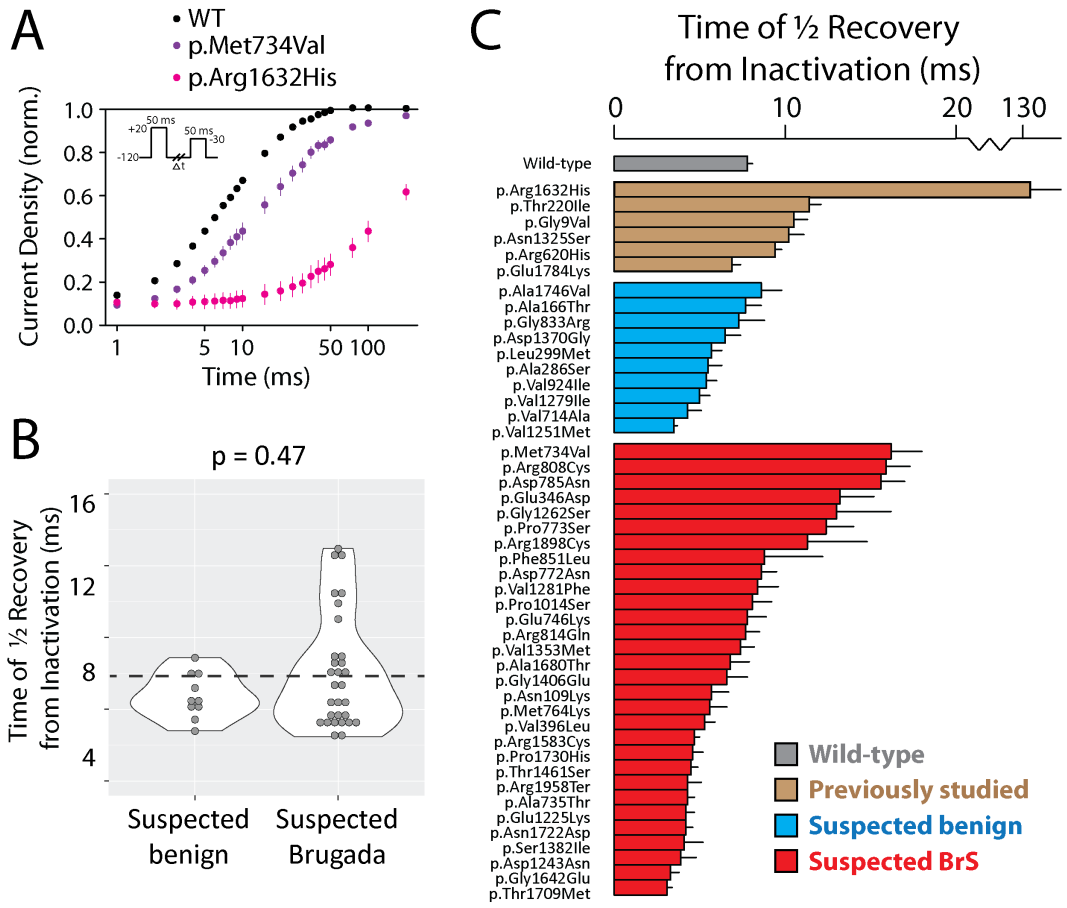

A) Normalized recovery inactivation curves for wild-type, p.Met734Val, the suspected Brugada syndrome-associated variant with the largest increase in recovery from inactivation time, and p.Arg1632His, a previously studied variant that has a very large recovery from inactivation.[3] Error bars indicate standard error of the mean. B) Violin plot of time of ½ recovery from inactivation, derived from fitting an exponential fit to the data derived from each cell. Black line indicates wild-type value. C) Barplot of wild-type (grey), previously studied (brown), suspected benign (blue), or suspected Brugada Syndrome-associated time of ½ recovery from inactivation. The X-axis has a break to accommodate the large value for p.Arg1632His. Bars

indicate mean +/- standard errors. Only variants with at least 5 qualifying cells were included, so most severe loss of function variants are not included.

Figure S10: Late current

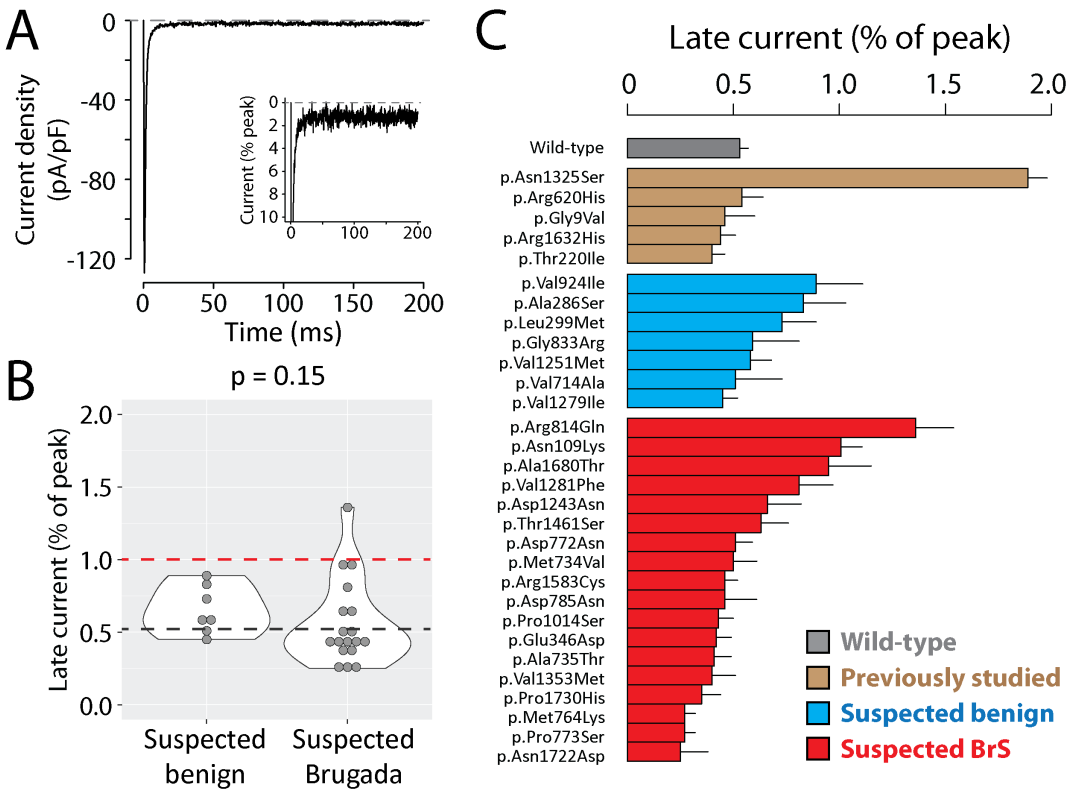

A) Tetracaine-sensitive late currents for p.Arg814Gln, the suspected Brugada syndrome-associated variant that has the largest observed increase in late current. B) Violin plot of time of late current (normalized as the percentage of peak current). Black line indicates wild-type value and red line indicates the cutoff (1%) that was considered to be deleterious. C) Barplot of wild-type (grey), previously studied (brown), suspected benign (blue), or suspected Brugada Syndrome-associated late current (normalized as the percentage of peak current). Bars indicate mean +/- standard errors. Only variants with at least 5 qualifying cells were included, so most severe loss of function variants are not included.

Figure S11. Partial rescue of loss of function variants

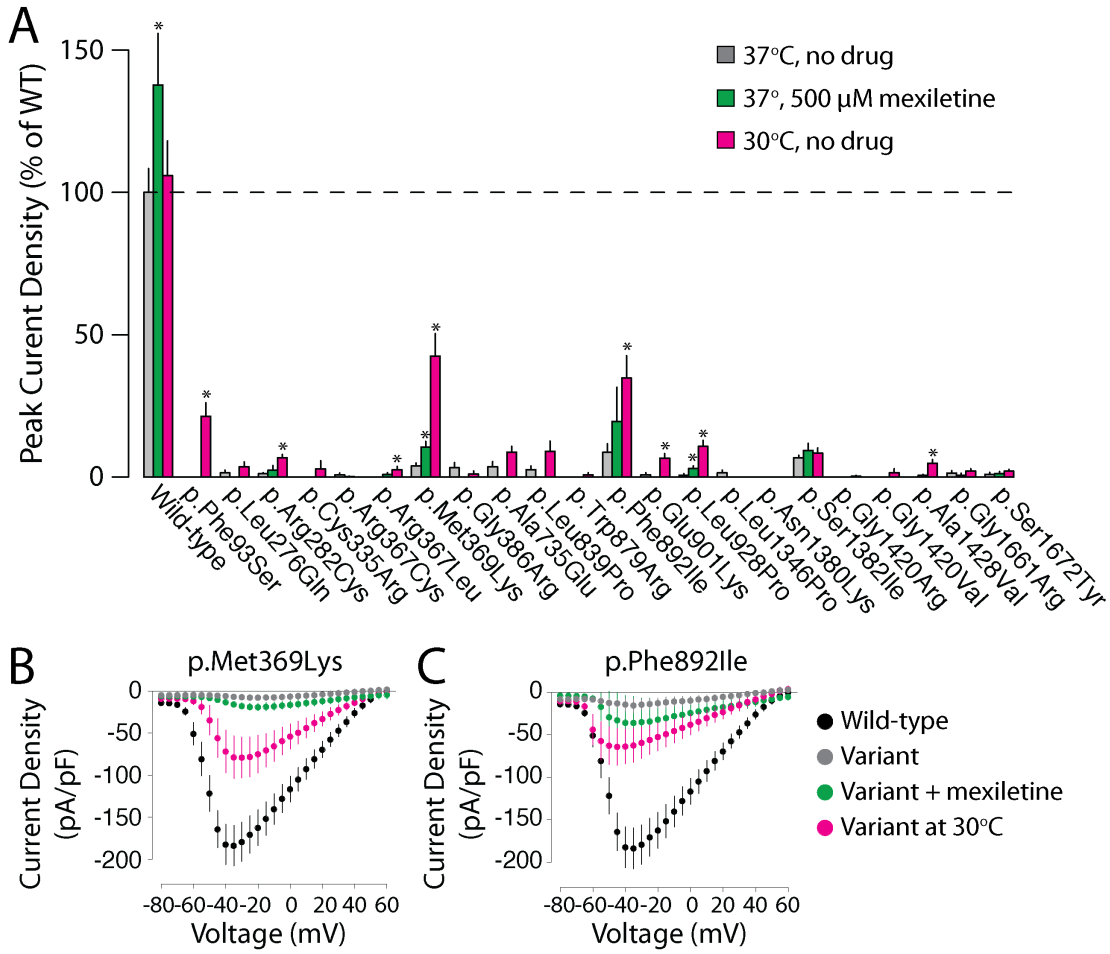

A) Peak current densities (normalized to wild-type-expressing cells from the same transfection) for the 22 variants with peak current densities <10% of wild-type. Variants were tested under usual conditions (37°, no drug, grey), with 24 hr of treatment with 500 µM mexiletine (green), or with 24 hr culture at 30° (pink). Values are mean ± standard error. *P<0.05, 2-tailed *t*-test compared with wild-type at 37° with no drug. 8/22 variants had significant increases in current at 30° and 2/22 variants had significant increases in mexiletine. B, C) Current-voltage plots for p.Met369Lys and p.Phe892Ile, the two variants with the largest response to 30°. Colors are the same as A), with black indicating wild-type at 37° with no drug.

Figure S12: Variant distance from the pore is strongly correlated with normalized peak current density

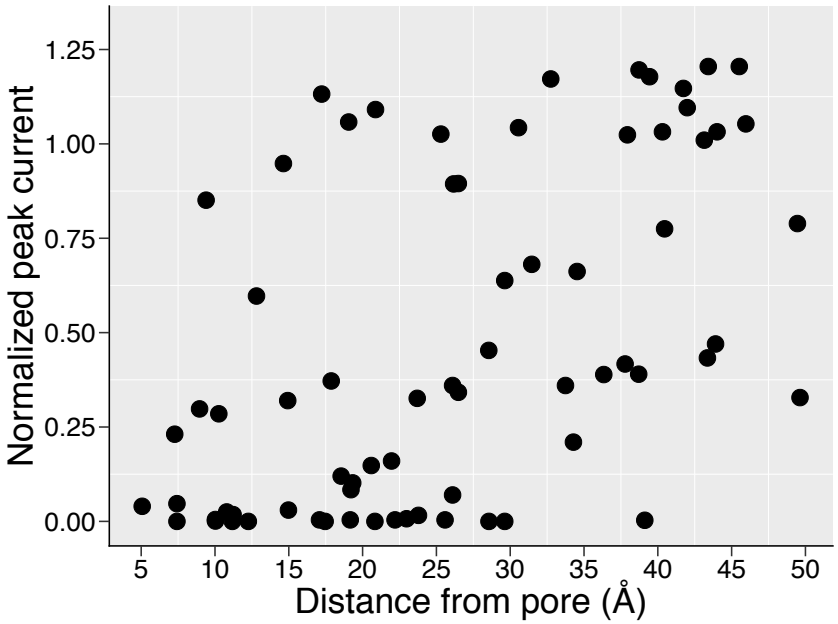

A scatter plot showing the correlation between variant distance from the pore and normalized peak currents (Pearson's $r = 0.54$, $p = 1.3\text{e} - 6$).

Figure S13. Estimated variant-induced change in thermostability is correlated with functional impact.

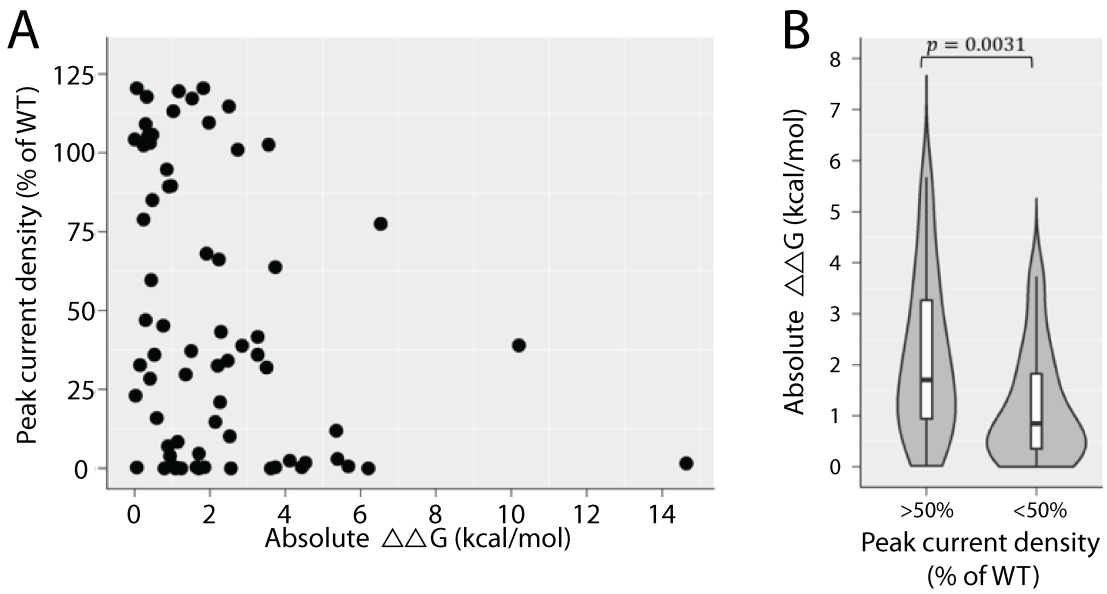

(A) A scatter plot showing the correlation between variant-induced perturbation to native thermostability (|ΔΔG|) and normalized peak currents (Pearson's $r = -0.31$, $p = 0.0092$). (B) A violin plot illustrating the distribution of absolute ΔΔG values of variants affecting SCN5A function (normalized peak current <50%, $n = 44$, median $|\Delta\Delta G| = 2.00\ kcal/mol$) and normal variants (normalized peak current >=50%, n=26 median $|\Delta\Delta G| = 0.88\ kcal/mol$, Mann-Whitney U test, $p = 0.0031$).

Figure S14. Variants may compromise function by disrupting the pore

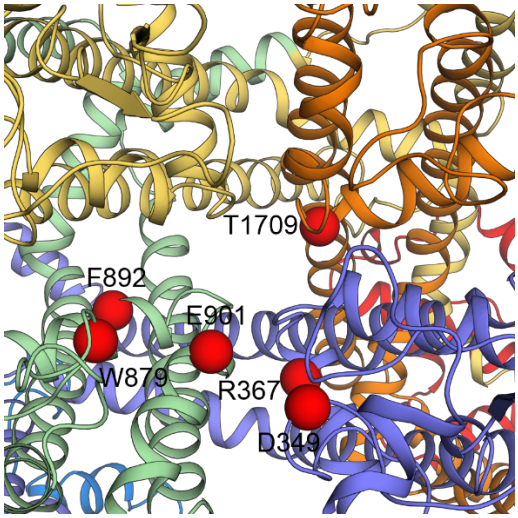

Seven pore-lining variants evaluated in this work, namely p.Asp349Asn, p.Arg367Cys, p.Arg367Leu, p.Trp879Arg, p.Phe892Ile, p.Glu901Lys, and p.Thr1709Met, cause (partial) loss of function (<50% peak current), potentially by disrupting the pore. These variants induce only minor changes in perturbations to native thermostability. The absolute ΔΔG values of these seven variants are 0.41, 1.06, 1.21, 1.09, 0.79, 0.94, 0.03 kcal/mol and the normalized peak currents are 0.29, 0.01, 0.00, 0.00, 0.00, 0.04, and 0.23, respectively. Domains are color coded as in Fig. S4. The Cα atoms of mutated residues are rendered as red spheres. p.Glu901Lys is further highlighted in Figure 5D.

Table S1. Literature and gnomAD counts, peak current density, and classifications

Class	Variant	BrS1	LQT3	Unaff.	gnomAD v2.1	Peak Curr. Density (% of WT)	ACMG Classification	
							Pre	Post
Wild-type	WT	*	*	*	*	100 (3.7)	*	*
Previously Studied	p.Gly9Val	0	1	0	0	115.6 (24.7)	VUS	VUS
	p.Arg121Trp	3	0	0	0	0.7 (0.6)	LP	LP
	p.Thr220Ile	2	0	2	197	86.7 (8.6)	VUS	VUS
	p.Thr353Ile	5	0	0	0	0.1 (0.1)	P	P
	p.Arg620His	1	0	3	7	113 (28.6)	B	B
	p.Gly752Arg	8	0	1	1	23.2 (7.1)	P	P
	p.Asn1325Ser	0	23	0	0	114.3 (22.4)	P(LQT)	P(LQT)
	p.Arg1432Gly	1	0	0	0	2.2 (1)	LP	LP
	p.Arg1632His	10	0	3	2	64.8 (11.1)	P	P
	p.Glu1784Lys	31	114	19	0	51.9 (18.8)	P(LQT +BrS)	P(LQT +BrS)
Suspected Benign	p.Ala166Thr	0	0	0	70	103.2 (21.8)	VUS	B
	p.Ala286Ser	0	0	1	79	105.8 (12.7)	LB	B
	p.Leu299Met	0	0	1	59	104.3 (16.3)	LB	B
	p.Val714Ala	0	0	0	16	101 (8.9)	VUS	B
	p.Gly833Arg	0	0	0	37	109.1 (14.8)	VUS	B
	p.Val924Ile	0	0	2	31	94.8 (12.6)	VUS	LB
	p.Val1251Met	0	0	1	59	120.5 (13.6)	VUS	B
	p.Val1279Ile	0	0	2	27	103.2 (12.7)	VUS	B
	p.Asp1370Gly	0	0	0	15	85.1 (10.6)	VUS	B
	p.Ala1746Val	0	0	0	15	89.4 (12.7)	VUS	B
Suspected Brugada Syndrome associated	p.Asp84Asn	2	0	0	0	32.8 (5)	VUS	LP
	p.Phe93Ser	2	0	0	0	0.2 (0.2)	VUS	LP
	p.Asn109Lys	3	0	0	1	119.6 (19.5)	VUS	LB
	p.Leu136Pro	2	0	0	0	39 (6.4)	VUS	LP
	p.Lys175Asn	1	0	0	0	117.8 (14.5)	VUS	VUS
	p.Ala178Gly	1	0	0	0	109.6 (19.8)	VUS	VUS
	p.Val223Leu	2	0	0	0	34.2 (6.7)	VUS	LP
	p.Leu276Gln	2	0	0	0	0.8 (0.6)	VUS	LP
	p.Arg282Cys	2	0	1	0	1.3 (0.3)	LP	P
	p.Cys335Arg	2	0	0	0	0 (0)	VUS	LP
	p.Glu346Asp	1	0	0	0	113.2 (13.9)	VUS	LB
	p.Asp349Asn	4	0	1	4	28.5 (7.6)	VUS	LP
	p.Arg367Cys	1	0	0	0	0 (0)	LP	P
	p.Arg367Leu	3	2	0	3	0.6 (0.4)	LP	P
	p.Met369Lys	3	0	0	0	3.4 (0.8)	VUS	LP
	p.Gly386Arg	2	0	0	0	1.2 (0.7)	VUS	LP
	p.Val396Leu	1	0	0	0	32 (5)	VUS	LP
	p.Met734Val	1	0	0	0	68.1 (8.7)	VUS	VUS
	p.Ala735Glu	2	0	0	0	0.9 (0.6)	VUS	LP
	p.Ala735Thr	3	0	1	0	63.8 (10.1)	VUS	VUS
	p.Glu746Lys	4	0	0	6	41.7 (10.8)	VUS	LP
	p.Met764Lys	2	0	0	0	77.5 (8.6)	VUS	VUS
	p.Asp772Asn	1	1	0	5	105.3 (10.8)	VUS	VUS
	p.Pro773Ser	1	0	0	0	120.5 (10.5)	VUS	VUS
	p.Asp785Asn	2	0	0	0	38.9 (7.2)	VUS	LP
	p.Arg808Cys	3	0	0	2	21 (5.1)	VUS	LP
	p.Arg814Gln	5	2	8	7	117.2 (11.7)	LP (BrS)	LP (LQT)

Suspected Brugada Syndrome associated	p.Leu839Pro	4	0	1	0	2.9 (2.1)	VUS	LP
	p.Phe851Leu	2	0	0	2	16 (2.3)	VUS	LP
	p.Trp879Arg	2	0	0	0	0 (0)	VUS	LP
	p.Phe892Ile	2	0	0	0	0.8 (0.6)	VUS	LP
	p.Glu901Lys	6	0	0	0	3.2 (0.5)	LP	P
	p.Asn927Ser	4	0	0	0	29.8 (5.7)	VUS	LP
	p.Leu928Pro	1	0	0	0	1.1 (0.8)	VUS	LP
	p.Pro1014Ser	2	0	0	0	121.4 (13.2)	VUS	LB
	p.Glu1225Lys	11	1	1	1	36 (5.9)	LP	P
	p.Asp1243Asn	5	0	1	41	114.7 (15.2)	VUS	B
	p.Gly1262Ser	4	0	0	8	47 (15.5)	VUS	VUS
	p.Val1281Phe	2	0	0	0	102.4 (15.5)	VUS	VUS
	p.Trp1345Cys	3	0	0	0	12 (2.2)	VUS	LP
	p.Leu1346Pro	2	0	0	0	1.6 (0.7)	VUS	LP
	p.Val1353Met	2	0	1	7	102.6 (16.5)	VUS	B
	p.Asn1380Lys	2	0	0	0	0.2 (0.2)	VUS	LP
	p.Ser1382Ile	3	0	5	0	3.5 (0.8)	VUS	LP
	p.Val1405Leu	2	0	0	0	13.9 (2.8)	VUS	LP
	p.Val1405Met	3	0	0	0	36 (6)	VUS	LP
	p.Gly1406Glu	2	0	0	0	32.6 (6.2)	LP	P
	p.Gly1420Arg	2	0	0	0	0 (0)	VUS	LP
	p.Gly1420Val	3	0	0	0	3 (1.5)	VUS	LP
	p.Ala1428Val	4	0	2	0	0.3 (0.3)	LP	P
	p.Tyr1449Cys	5	0	4	0	10.2 (3.4)	LP	P
	p.Thr1461Ser	2	0	2	0	59.7 (6.3)	VUS	VUS
	p.Glu1574Lys	4	0	0	0	43.3 (12.2)	VUS	LP
	p.Arg1583Cys	2	0	0	2	78.9 (7.2)	VUS	VUS
	p.Gly1642Glu	1	0	0	0	14.8 (2.5)	VUS	LP
	p.Gly1661Arg	7	0	0	0	5.4 (1.5)	LP	P
	p.Ser1672Tyr	3	0	0	0	0.9 (0.5)	VUS	LP
	p.Ala1680Thr	4	1	0	13	89.5 (14.6)	VUS	B
	p.Thr1709Met	2	1	0	1	23.1 (3.2)	VUS	LP
	p.Asn1722Asp	3	0	5	0	37.2 (3.8)	VUS	LP
	p.Pro1730His	2	0	3	0	45.3 (5.1)	VUS	LP
	p.Arg1898Cys	2	0	1	10	28.4 (8.6)	VUS	LP
	p.Arg1958Ter	0	2	0	13	59.3 (8.3)	VUS	VUS

Peak current density is normalized to WT and presented as mean (standard error).

VUS=Variant of Uncertain Significance, P=Pathogenic, LP=Likely Pathogenic, B=Benign, LB=Likely Benign. Susp. BrS = Suspected BrS, Susp. Benign = Suspected Benign, Unaff.=Unaffected, Peak curr. Density=Peak Current Density. Counts of individuals with or without disease are from a literature curation of *SCN5A* variants.[4,5] Variant classifications are for Brugada Syndrome unless otherwise indicated.

Table S2. Zone boundaries and restriction enzymes

Zone	Size (bp)	Location (bp)	Restriction enzymes
1	727	1-727	AgeI, BssHII
2	835	722-1557	BssHII, SpeI
3	683	1552-2235	SpeI, EcoRI
4	757	2230-2987	EcoRI, NheI
5	829	2982-3811	NheI, NsiI
6	790	3806-4596	NsiI, AatII
7	769	4591-5360	AatII, AflII
8	704	5355-6059	AflII, NdeI

Zone locations are slightly overlapping because each restriction enzyme site is present in two adjacent zone plasmids. Coordinates refer to the canonical numbering scheme with Gln1077 included (ENST00000333535), although the wild-type plasmid used in this study had Gln1077 deleted (ENST00000443581).

Table S3. Primers used in this study

Variant	Zone	Name	Sequence
p.Gly9Val	1	ag654	CCTATTACCTCGGGTCACCAGCAGCTTCC
p.Asp84Asn	1	ag737	CCCTGGAGGACCTGAACCCCTTCTATAGC
p.Phe93Ser	1	ag738	CTATAGCACCCAAAAGACTTCCATCGTACTGAATAAAGGCA
p.Asn109Lys	1	ag739	TTCCGGTTCAGTGCCACCAAAGCCTTGTATGTC
p.Arg121Trp	1	ag655	CTTCCACCCCATCTGGAGAGCGGCTGT
p.Leu136Pro	1	ag740	CTCGCTCTTCAACATGCCCATCATGTGCACCATCC
p.Ala166Thr	1	ag656	TCGAGTACACCTTCACCACCATTTACACCTTTGAG
p.Lys175Asn	1	ag775	TGAGTCTCTGGTCAACATTCTGGCTCGAGGC
p.Ala178Gly	1	ag776	GGTCAAGATTCTGGGTCGAGGCTTCTGCC
p.Thr220Ile	1	ag728	CTCAGCCTTACGCATCTTCCGAGTCCTCC
p.Val223Leu	1	ag741	CCTTACGCACCTTCCGACTCCTCCGGG
p.Leu276Gln	2	ag742	CTCTTCATGGGCAACCAAAGGCACAAGTGCGTG
p.Arg282Cys	2	ag729	GGCACAAGTGCGTGTGCAACTTCACAGCG
p.Ala286Ser	2	ag660	GTGCGTGCGCAACTTCACATCGCTCAACGG
p.Leu299Met	2	ag661	GGAGGCCGACGGCATGGTCTGGGAATC
p.Cys335Arg	2	ag785	GACGCTGGGACACGTCCGGAGGGCT
p.Glu346Asp	2	ag777	TAAAGGCAGGCGACAACCCCGACCACG
p.Asp349Asn	2	ag786	AGGCGAGAACCCCAACCACGGCTACAC
p.Thr353Ile	2	ag664	CCGACCACGGCTACATCAGCTTCGATTCCTT
p.Arg367Cys	2	ag778	TTTCTTGCACTCTTCCTCCTGATGACGCAGGAC
p.Arg367Leu	2	ag665	CTTTCTTGCACTCTTCTGCCTGATGACGCAGGA
p.Met369Lys	2	ag743	CTCTTCCGCCTGAAGACGCAGGACTGC
p.Gly386Arg	2	ag745	AGACCCTCAGGTCCGCAAGGAAGATCTACATG
p.Val396Leu	2	ag779	CATGATCTTCTTCATGCTTCTCATCTTCCTGGGGTC
p.Arg620His	3	ag128	AAGCCACCTCCTCCACCCTGTGATGCTAG
p.Val714Ala	3	ag691	GGAGTGAAGTTGGTGGCCATGGACCCGTTTACT
p.Met734Val	3	ag780	CTCAACACACTCTTCGTGGCGCTGGAGCACT
p.Ala735Glu	3	ag746	CAACACACTCTTCATGGAGCTGGAGCACTACAACA
p.Ala735Thr	3	ag747	TCAACACACTCTTCATGACGCTGGAGCACTACAAC
p.Glu746Lys	4	ag669	GCGGCCGCGAATTCAAGGAGATGCTGCA
p.Gly752Arg	4	ag145	GGAGATGCTGCAGGTCAGAAACCTGGTCTTCAC
p.Met764Lys	4	ag790	GGATTTTCACAGCAGAGAAGACCTTCAAGATCATTGC
p.Asp772Asn	4	ag670	TCAAGATCATTGCCCTCAACCCCTACTACTACTTC
p.Pro773Ser	4	ag781	AGATCATTGCCCTCGACTCCTACTACTACTTCCAA
p.Asp785Asn	4	ag748	AGGGCTGGAACATCTTCAACAGCATCATCGTCATC
p.Arg808Cys	4	ag672	CTTGTCGGTGCTGTGCTCCTTCCGCCT
p.Arg814Gln	4	ag674	CTTCCGCCTGCTGCAGGTCTTCAAGCTGG
p.Gly833Arg	4	ag675	ACTCATCAAGATCATCAGGAACTCAGTGGGGGC
p.Leu839Pro	4	ag749	CAGTGGGGGCACCGGGGAACCTGAC
p.Phe851Leu	4	ag799	TGCTTGCCATCATCGTGCTCATCTTTGCTGTGGTG
p.Trp879Arg	4	ag798	CCTGCTGCCTCGCAGGCACATGATGGA
p.Phe892Ile	4	ag750	GCCTTCCTCATCATCATCCGCATCCTCTGTG
p.Glu901Lys	4	ag678	CTGTGGAGAGTGGATCAAGACCATGTGGGACTG
p.Val924Ile	4	ag680	TGGTCTTCTTGCTTGTTATGATCATTGGCAACCTTGTGGTC
p.Asn927Ser	4	ag751	CTTGTTATGGTCATTGGCAGCCTTGTGGTCCTGAAT
p.Leu928Pro	4	ag782	TATGGTCATTGGCAACCCTGTGGTCCTGAATCTCT
p.Pro1014Ser	5	ag792	CCCCGCCACCCTCAGAGACGGAG
p.Glu1225Lys	5	ag687	GGAGCGCTGGCCTTCAAGGACATCTACCTAG
p.Asp1243Asn	5	ag688	GGTTCTGCTTGAGTATGCCAACAAGATGTTCACATATGT
p.Val1251Met	5	ag689	TGTTCACATATGTCTTCATGCTGGAGATGCTGCTC
p.Gly1262Ser	5	ag690	TCAAGTGGGTGGCCTACAGCTTCAAGAAGTACTTC

p.Val1279Ile	6	ag704	GCTCGACTTCCTCATCATAGATGTCTCTCTGGT
p.Val1281Phe	6	ag752	CTTCCTCATCGTAGACTTCTCTCTGGTCAGCCT
p.Asn1325Ser	6	ag132	GGCATGAGGGTGGTGGTCAGTGCCCTGGTG
p.Trp1345Cys	6	ag753	GTCTGCCTCATCTTCTGCCTCATCTTCAGCATCAT
p.Leu1346Pro	6	ag754	CTGCCTCATCTTCTGGCCCATCTTCAGCATCATGG
p.Val1353Met	6	ag697	CTTCAGCATCATGGGCATGAACCTCTTTGCGGG
p.Asp1370Gly	6	ag698	CAACCAGACAGAGGGAGGCTTGCCTTTGAACTACA
p.Asn1380Lys	6	ag755	TTTGAACTACACCATCGTGAACAAAAAGAGCCAGTGTG
p.Ser1382Ile	6	ag795	CTACACCATCGTGAACAACAAGATCCAGTGTGAGTC
p.Val1405Leu	6	ag756	AGTCAACTTTGACAACCTGGGGGCCGGGTA
p.Val1405Met	6	ag757	AAAGTCAACTTTGACAACATGGGGGCCGGGTAC
p.Gly1406Glu	6	ag758	CTTTGACAACGTGGAGGCCGGGTACCTGG
p.Gly1420Arg	6	ag759	GTCCATCCAGCGTTTAAATGTTGCCACCTGCAG
p.Gly1420Val	6	ag760	GCAGGTGGCAACATTTAAAGTCTGGATGGACATTATGTATG
p.Ala1428Val	6	ag761	GGACATTATGTATGCAGTTGTGGACTCCAGGGGG
p.Arg1432Gly	6	ag783	CAGCTGTGGACTCCGGGGGGTATGAAGAG
p.Tyr1449Cys	6	ag762	ACCTCTACATGTACATCTGTTTTGTCATTTTCATCAT
p.Thr1461Ser	6	ag796	CATCTTTGGGTCTTTCTTCTCCCTGAACCTCTTTATTGG
p.Glu1574Lys	7	ag764	TGGCCATCTTCACAGGCAAGTGTATTGTCAAGCTG
p.Arg1583Cys	7	ag794	AGCTGGCTGCCCTGTGCCACTACTACTTC
p.Arg1632His	7	ag642	GGCCCGAATAGGCCACATCCTCAGACTGA
p.Gly1642Glu	7	ag784	GAGGGGCCAAGGAGATCCGCACGCT
p.Gly1661Arg	7	ag645	GCCCTCTTCAACATCAGGCTGCTGCTCTTCC
p.Ser1672Tyr	7	ag766	CGTCATGTTCATCTACTACATCTTTGGCATGGCCA
p.Ala1680Thr	7	ag646	TTGGCATGGCCAACTTCACTTATGTCAAGTGGGAG
p.Thr1709Met	7	ag797	TTCCAGATCACCATGTCGGCCGGCTGG
p.Asn1722Asp	7	ag791	AGCCCCATCCTCGACACTGGGCCGC
p.Pro1730His	7	ag793	CCCTACTGCGACCACACTCTGCCCAAC
p.Ala1746Val	7	ag650	CGGGAGCCCAGTCGTGGGCATCC
p.Glu1784Lys	7	ag653	GGAGGAGAGCACCAAGCCCTTAAGGCG
p.Arg1898Cys	8	ag700	CCACCACACTCCGGTGCAAGCACGAAGAG
p.Arg1958Ter	8	ag734	GTGAGAACTTCTCCTGACCCCTTGGCCCA

Table S4. Reasons for cell exclusion

Parameter	Candidate cells	Inclusion criteria	Cells meeting inclusion	Good fitting best fit curve	Post-outlier removal (final)
$V_{1/2}$ activation	2010	100-2000 pA	1645	1256	1250
$V_{1/2}$ inactivation	2010	100-2000 pA	1645	1188	1150
Inactivation time	2010	100-2000 pA	1645	1440	1413
Recovery from inactivation	2010	100-2000 pA	1645	1005	1005
Late current	2010	500-2000 pA, <10% change in seal resistance/capacitance	577	577	566

Table S5. ACMG criteria used for variant classification

Class	Variant	Criteria	PS3/BS3	ACMG (Pre)	ACMG (Post)
Suspected Benign	p.Ala166Thr	PP2 BS1	BS3	VUS	B
	p.Ala286Ser	PP2 BS1 BP4	BS3	LB	B
	p.Leu299Met	PP2 BS1 BP4	BS3	LB	B
	p.Val714Ala	PP2 BS1	BS3	VUS	B
	p.Gly833Arg	PP2 PP3 BS1	BS3	VUS	B
	p.Val924Ile	PM2 PP2 BP4	BS3	VUS	LB
	p.Val1251Met	PP2 BS1	BS3	VUS	B
	p.Val1279Ile	PP2 BS1	BS3	VUS	B
	p.Asp1370Gly	PP2 BS1	BS3	VUS	B
	p.Ala1746Val	PP2 BS1	BS3	VUS	B
Suspected Brugada-associated	p.Asp84Asn	PM2 PP2 PP3	PS3	VUS	LP
	p.Phe93Ser	PM2 PP2 PP3	PS3	VUS	LP
	p.Asn109Lys	PM2 PP2 BP4	BS3	VUS	LB
	p.Leu136Pro	PM2 PP2	PS3	VUS	LP
	p.Lys175Asn	PM2 PP2 PP3	BS3	VUS	VUS
	p.Ala178Gly	PM2 PP2 PP3	BS3	VUS	VUS
	p.Val223Leu	PM2 PP2 PP3	PS3	VUS	LP
	p.Leu276Gln	PM2 PP2 PP3	PS3	VUS	LP
	p.Arg282Cys	PM2 PM5 PP2 PP3 PP5	PS3	LP	P
	p.Cys335Arg	PM2 PP2 PP3	PS3	VUS	LP
	p.Glu346Asp	PM2 PP2 BP4	BS3	VUS	LB
	p.Asp349Asn	PM2 PP2	PS3	VUS	LP
	p.Arg367Cys	PM2 PM5 PP2 PP3	PS3	LP	P
	p.Arg367Leu	PM2 PM5 PP2 PP3 PP5	PS3	LP	P
	p.Met369Lys	PM2 PP2 PP3	PS3	VUS	LP
	p.Gly386Arg	PM2 PP2 PP3	PS3	VUS	LP
	p.Val396Leu	PM2 PP2 PP3	PS3	VUS	LP
	p.Met734Val	PM2 PP2	*	VUS	VUS
	p.Ala735Glu	PM2 PM5 PP2	PS3	VUS	LP
	p.Ala735Thr	PM2 PM5 PP2	*	VUS	VUS
	p.Glu746Lys	PM2 PP2 BP4	PS3	VUS	LP
	p.Met764Lys	PM2 PP2	BS3	VUS	VUS
	p.Asp772Asn	PM2 PP2	BS3	VUS	VUS
	p.Pro773Ser	PM2 PP2	BS3	VUS	VUS
	p.Asp785Asn	PM2 PP2 PP3	PS3	VUS	LP
	p.Arg808Cys	PM2 PP2 PP3	PS3	VUS	LP
	p.Arg814Gln	PS4 PP2 PP3 BS1	PS3 (LQT)	LP (BrS)	LP (LQT)
	p.Leu839Pro	PM2 PP2 PP3	PS3	VUS	LP
	p.Phe851Leu	PM2 PP2 PP3	PS3	VUS	LP
	p.Trp879Arg	PM2 PP2 PP3	PS3	VUS	LP
	p.Phe892Ile	PM2 PP2	PS3	VUS	LP
	p.Glu901Lys	PS4 PM2 PP2 PP3	PS3	LP	P
	p.Asn927Ser	PM2 PP2	PS3	VUS	LP
	p.Leu928Pro	PM2 PP2	PS3	VUS	LP
	p.Pro1014Ser	PM2 PP2 BP4	BS3	VUS	LB

Suspected Brugada-associated	p.Glu1225Lys	PS4 PM2 PP2 PP3	PS3	LP	P
	p.Asp1243Asn	PP2 PP3 BS1	BS3	VUS	B
	p.Gly1262Ser	PP2 PP3 BS1	*	VUS	VUS
	p.Val1281Phe	PM2 PP2 PP3	BS3	VUS	VUS
	p.Trp1345Cys	PM2 PP2 PP3	PS3	VUS	LP
	p.Leu1346Pro	PM2 PP2 PP3	PS3	VUS	LP
	p.Val1353Met	PP2 PP3 BS1	BS3	VUS	B
	p.Asn1380Lys	PM2 PP2 PP3	PS3	VUS	LP
	p.Ser1382Ile	PM2 PP2 PP3	PS3	VUS	LP
	p.Val1405Leu	PM2 PP2 PP3	PS3	VUS	LP
	p.Val1405Met	PM2 PP2 PP3	PS3	VUS	LP
	p.Gly1406Glu	PM2 PM5 PP2 PP3	PS3	LP	P
	p.Gly1420Arg	PM2 PP2 PP3	PS3	VUS	LP
	p.Gly1420Val	PM2 PP2 PP3	PS3	VUS	LP
	p.Ala1428Val	PM2 PM5 PP2 PP3	PS3	LP	P
	p.Tyr1449Cys	PS4 PM2 PP2 PP3 PP5	PS3	LP	P
	p.Thr1461Ser	PM2 PP2	*	VUS	VUS
	p.Glu1574Lys	PM2 PP2 PP3	PS3	VUS	LP
	p.Arg1583Cys	PM2 PP2 PP3	BS3	VUS	VUS
	p.Gly1642Glu	PM2 PP2 PP3	PS3	VUS	LP
	p.Gly1661Arg	PS4 PM2 PP2 PP3	PS3	LP	P
	p.Ser1672Tyr	PM2 PP2 PP3	PS3	VUS	LP
	p.Ala1680Thr	PP2 PP3 BS1	BS3	VUS	B
	p.Thr1709Met	PM2 PP2 PP3	PS3	VUS	LP
	p.Asn1722Asp	PM2 PP2 PP3	PS3	VUS	LP
	p.Pro1730His	PM2 PP2 PP3	PS3	VUS	LP
	p.Arg1898Cys	PP2 PP3 BS1	PS3	VUS	LP
	p.Arg1958Ter	PM4	*	VUS	VUS

American College of Medical Genetics (ACMG) criteria were adapted from Richards et al[1] as described in the methods. ACMG (Pre) and ACMG (Post) indicate the ACMG classification before and after patch clamp data from this study are included, respectively.

Table S6. Summary of the Rosetta energy functions used for $\Delta\Delta G$ calculation

Energy term	Weight	Description
fa_atr	0.18	Lennard-Jones attractive between atoms in different residues
fa_dun	0.07	Internal energy of sidechain rotamers as derived from Dunbrack's statistics
fa_mbenv	0.17	Statistics-based depth-dependent membrane environment potential
fa_mpsolv	0.23	Statistics-based depth- and burial-dependent solvation potential
fa_pair	0.57	Statistics-based amino-acid pair potential, favors salt bridges
fa_rep	0.08	Lennard-Jones repulsive between atoms in different residues
hbond_bb_sc	0.45	Sidechain-backbone hydrogen bond energy
hbond_sc	0.43	Sidechain-sidechain hydrogen bond energy
omega	0.09	Omega dihedral in the backbone. A harmonic constraint on planarity with standard deviation of ~6 degrees

Table S7. All measured parameters for each variant

Variant	n	Peak density	V1/2 Activation	Inact. time	V1/2 Inactivation	Rec. from Inactivation	Late (% peak)
WT	471	100 (3.7)	-36.8 (0.6)	2 (0)	-95.5 (0.4)	7.8 (0.3)	0.53 (0.04)
p.Gly9Val	19	115.6 (24.7)	-40.2 (1.1)	1.8 (0.1)	-100.6 (1.3)	10.5 (0.8)	0.46 (0.14)
p.Arg121Trp	17	0.7 (0.6)	*	*	*	*	*
p.Thr220Ile	28	86.7 (8.6)	-39.5 (2)	2 (0.1)	-99.2 (1)	11.4 (0.7)	0.4 (0.06)
p.Thr353Ile	19	0.1 (0.1)	*	*	*	*	*
p.Arg620His	17	113 (28.6)	-44.1 (1.3)	1.9 (0.2)	-98.2 (1.4)	9.4 (0.4)	0.54 (0.1)
p.Gly752Arg	14	23.2 (7.1)	-14.2 (2.4)	*	*	*	*
p.Asn1325Ser	16	114.3 (22.4)	-46.4 (1.4)	2.2 (0.1)	-98.7 (1.9)	10.2 (0.9)	1.89 (0.09)
p.Arg1432Gly	16	2.2 (1)	*	*	*	*	*
p.Arg1632His	31	64.8 (11.1)	-47.7 (2.1)	2.7 (0.2)	-107.5 (3.9)	133.9 (13)	0.44 (0.07)
p.Glu1784Lys	12	51.9 (18.8)	*	1.4 (0.2)	-100.9 (3.7)	6.9 (0.5)	*
p.Ala166Thr	37	103.2 (21.8)	-32.6 (1.9)	2.7 (0.3)	-104 (1.9)	7.7 (0.9)	*
p.Ala286Ser	36	105.8 (12.7)	-33.6 (1.4)	2.3 (0.2)	-92.8 (0.9)	5.5 (0.8)	0.83 (0.2)
p.Leu299Met	30	104.3 (16.3)	-31.6 (1.8)	3 (0.3)	-92.9 (1.2)	5.7 (0.6)	0.73 (0.16)
p.Val714Ala	41	101 (8.9)	-30.6 (1.2)	2.5 (0.1)	-90.6 (1.2)	4.3 (0.8)	0.51 (0.22)
p.Gly833Arg	26	109.1 (14.8)	-35.5 (1.9)	2.2 (0.2)	-93.3 (1)	7.3 (1.5)	0.59 (0.22)
p.Val924Ile	33	94.8 (12.6)	-31.6 (1.7)	2.2 (0.2)	-90.8 (1)	5.4 (0.6)	0.89 (0.22)
p.Val1251Met	33	120.5 (13.6)	-31.9 (1.2)	2.5 (0.1)	-91.1 (1.2)	3.5 (0.2)	0.58 (0.1)
p.Val1279Ile	33	103.2 (12.7)	-30.9 (1.7)	2.5 (0.2)	-92.8 (1)	5 (0.6)	0.45 (0.07)
p.Asp1370Gly	35	85.1 (10.6)	-30.6 (1.4)	2.5 (0.2)	-94.7 (1.5)	6.5 (0.9)	*
p.Ala1746Val	26	89.4 (12.7)	-35.4 (2.6)	2.5 (0.1)	-92.2 (1.3)	8.6 (1.2)	*
p.Asp84Asn	16	32.8 (5)	-28.9 (3.1)	3.1 (1.2)	*	*	*
p.Phe93Ser	15	0.2 (0.2)	*	*	*	*	*
p.Asn109Lys	22	119.6 (19.5)	-38.2 (2.6)	2.5 (0.2)	-94.2 (1.5)	5.7 (1)	0.98 (0.1)
p.Leu136Pro	16	39 (6.4)	*	3.3 (0.7)	*	*	*
p.Lys175Asn	15	117.8 (14.5)	-29.5 (3.8)	2.2 (0.2)	-104.6 (2.1)	*	*
p.Ala178Gly	11	109.6 (19.8)	-27.6 (1.6)	2.2 (0.3)	*	*	*
p.Val223Leu	14	34.2 (6.7)	-39.1 (2.9)	2.1 (0.1)	-98.5 (3)	*	*
p.Leu276Gln	14	0.8 (0.6)	*	*	*	*	*
p.Arg282Cys	67	1.3 (0.3)	*	2.6 (0.6)	*	*	*
p.Cys335Arg	24	0 (0)	*	*	*	*	*
p.Glu346Asp	30	113.2 (13.9)	-44.4 (3.2)	1.7 (0.1)	-99.6 (2.4)	13.2 (2)	0.42 (0.07)
p.Asp349Asn	21	28.5 (7.6)	-26.5 (3.1)	*	*	*	*
p.Arg367Cys	25	0.6 (0.4)	*	*	*	*	*
p.Arg367Leu	39	0 (0)	*	*	*	*	*
p.Met369Lys	22	3.4 (0.8)	*	*	*	*	*
p.Gly386Arg	11	1.2 (0.7)	*	*	*	*	*
p.Val396Leu	31	32 (5)	-33.5 (1.4)	2.9 (0.1)	-94.9 (1.3)	5.3 (0.6)	*
p.Met734Val	18	68.1 (8.7)	-36.1 (2.1)	1.6 (0.1)	-103.2 (1.4)	16.2 (1.8)	0.5 (0.11)
p.Ala735Glu	12	0.9 (0.6)	*	*	*	*	*
p.Ala735Thr	25	63.8 (10.1)	-31.4 (1.3)	2.4 (0.2)	-91.6 (0.7)	4.3 (0.4)	0.41 (0.08)
p.Glu746Lys	15	41.7 (10.8)	-36.3 (1.9)	2 (0.1)	-97 (1.4)	7.8 (1.1)	*
p.Met764Lys	30	77.5 (8.6)	-32.9 (2.1)	2.7 (0.2)	-92.5 (1.4)	5.6 (1)	0.27 (0.05)
p.Asp772Asn	41	105.3 (10.8)	-43 (2.5)	1.4 (0.1)	-96.2 (1.5)	8.6 (0.9)	0.51 (0.08)
p.Pro773Ser	41	120.5 (10.5)	-35.1 (1.7)	2.4 (0.1)	-99.3 (1.1)	12.4 (1.6)	0.27 (0.05)
p.Asp785Asn	27	38.9 (7.2)	-25 (1.5)	2.7 (0.3)	-102.6 (1.8)	15.6 (1.4)	0.46 (0.15)
p.Arg808Cys	12	21 (5.1)	-35.8 (1.9)	1.6 (0.1)	-104.1 (1.3)	15.9 (1.4)	*
p.Arg814Gln	36	117.2 (11.7)	-38.9 (1.5)	2.1 (0.1)	-95.7 (1.1)	7.7 (0.8)	1.36 (0.18)
p.Leu839Pro	20	2.9 (2.1)	*	*	*	*	*
p.Phe851Leu	26	16 (2.3)	-32.5 (1.5)	1.8 (0.1)	-95.8 (3.1)	8.8 (3.4)	*

p.Trp879Arg	43	0 (0)	*	*	*	*	*
p.Phe892Ile	23	0.8 (0.6)	*	*	*	*	*
p.Glu901Lys	16	3.2 (0.5)	-32.8 (3)	2.2 (0.4)	*	*	*
p.Asn927Ser	13	29.8 (5.7)	*	*	*	*	*
p.Leu928Pro	27	1.1 (0.8)	*	*	*	*	*
p.Pro1014Ser	34	121.4 (13.2)	-46.6 (1.8)	1.4 (0.1)	-95.9 (1.6)	8.1 (1.1)	0.43 (0.07)
p.Glu1225Lys	19	36 (5.9)	-32.9 (1.3)	2.4 (0.1)	-84 (1.5)	4.2 (0.5)	*
p.Asp1243Asn	42	114.7 (15.2)	-31.1 (1.5)	2.6 (0.1)	-87.7 (1.1)	3.9 (0.9)	0.66 (0.16)
p.Gly1262Ser	10	47 (15.5)	-49 (2.7)	2.3 (0.3)	-97.3 (5.3)	13 (3.2)	*
p.Val1281Phe	39	102.4 (15.5)	-39.6 (1.9)	2.5 (0.1)	-96.8 (1)	8.4 (1.2)	0.81 (0.16)
p.Trp1345Cys	10	12 (2.2)	*	*	*	*	*
p.Leu1346Pro	15	1.6 (0.7)	*	*	*	*	*
p.Val1353Met	31	102.6 (16.5)	-33 (2.3)	2.2 (0.2)	-94 (1.6)	7.4 (0.8)	0.4 (0.11)
p.Asn1380Lys	25	0.2 (0.2)	*	*	*	*	*
p.Ser1382Ile	29	3.5 (0.8)	-40.3 (4)	2.7 (0.6)	*	4.1 (1.1)	*
p.Val1405Leu	15	13.9 (2.8)	-39.4 (2.3)	1.4 (0.1)	-97.1 (3.2)	*	*
p.Val1405Met	14	36 (6)	-26.8 (2.1)	2 (0.3)	*	*	*
p.Gly1406Glu	10	32.6 (6.2)	-42.7 (1.6)	1.9 (0.2)	-98 (2.2)	6.6 (1.2)	*
p.Gly1420Arg	16	3 (1.5)	*	*	*	*	*
p.Gly1420Val	11	0 (0)	*	*	*	*	*
p.Ala1428Val	24	0.3 (0.3)	*	*	*	*	*
p.Tyr1449Cys	12	10.2 (3.4)	*	*	*	*	*
p.Thr1461Ser	41	59.7 (6.3)	-35.7 (1.3)	1.8 (0.1)	-92.5 (1)	4.5 (0.4)	0.63 (0.13)
p.Glu1574Lys	14	43.3 (12.2)	-27 (3.7)	*	*	*	*
p.Arg1583Cys	38	78.9 (7.2)	-39.5 (1.1)	1.8 (0.1)	-96.8 (0.7)	4.7 (0.3)	0.46 (0.06)
p.Gly1642Glu	27	14.8 (2.5)	-33 (1.3)	2.4 (0.2)	-88.9 (2)	3.3 (0.5)	*
p.Gly1661Arg	19	5.4 (1.5)	*	1.6 (0.2)	*	*	*
p.Ser1672Tyr	18	0.9 (0.5)	*	*	*	*	*
p.Ala1680Thr	29	89.5 (14.6)	-42.1 (2.6)	2.2 (0.1)	-96.7 (1.6)	6.8 (1.1)	0.95 (0.2)
p.Thr1709Met	33	23.1 (3.2)	-35.9 (1.3)	2.4 (0.1)	-91.8 (1.2)	3.1 (0.3)	*
p.Asn1722Asp	26	37.2 (3.8)	-29.9 (1.4)	3.3 (0.2)	-89.5 (0.8)	4.2 (0.4)	0.25 (0.13)
p.Pro1730His	31	45.3 (5.1)	-30.1 (1.7)	3.1 (0.2)	-88.2 (1.3)	4.6 (0.6)	0.35 (0.09)
p.Arg1898Cys	13	28.4 (8.6)	-44.4 (3.9)	1.6 (0.1)	-100.7 (1.8)	11.3 (3.5)	*
p.Arg1958Ter	30	59.3 (8.3)	-30.7 (1.7)	2.6 (0.1)	-93.7 (1.4)	4.3 (0.8)	*

This dataset is also available in File S1 in a .csv format. N indicates the total number of cells included for the peak current parameter. The number of analyzed cells for the other parameters are presented in File S1. Only variants with at least 5 qualifying cells were included for non-peak density parameters, so most severe loss of function variants are not included for most parameters.

Table S8. *SCN5A* missense variants with <10% peak current density

Variant	Location	Peak current (% of WT)		PMID	BrS1	LQT3	Unaff.	gnomAD v2.1
		This study	Previous literature					
p.Phe93Ser	N-terminus	0.2	*	*	2	0	0	0
p.Arg104Gln	N-terminus	*	0	23805106	5	0	0	0
p.Arg104Trp	N-terminus	*	0	22739120	2	0	0	1
p.Arg121Trp	N-terminus	0.7	0	20395683	3	0	0	0
p.Thr187Ile	DI S2-S3 linker	*	0	16325048	1	0	0	0
p.Leu276Gln	DI S5-P linker	0.8	*	*	2	0	0	0
p.Arg282Cys	DI S5-P linker	1.3	*	*	2	0	1	0
p.Arg282His	DI S5-P linker	*	5	21840964	4	0	0	4
p.Cys335Arg	DI S5-P linker	0	*	*	2	0	0	0
p.Thr353Ile	DI S5-P linker	0.1	8.3	17198989	5	0	0	0
p.Asp356Asn	DI S5-P linker	*	0	16325048	9	0	0	1
p.Arg367Cys	DI S5-P linker	0.6	*	*	3	2	0	3
p.Arg367Leu	DI S5-P linker	0	*	*	1	0	0	0
p.Met369Lys	DI S5-P linker	3.4	*	*	3	0	0	0
p.Gly386Arg	DI S6	1.2	*	*	2	0	0	0
p.Ala735Glu	DII S1	0.9	*	*	2	0	0	0
p.Gly752Arg	DII S2	23.2	6.3	12693506	8	0	1	1
p.Leu839Pro	DII S5	2.9	*	*	4	0	1	0
p.Leu846Arg	DII S5	*	0	22028457	1	0	0	0
p.Arg878Cys	DII S5-P linker	*	0	18616619	32	0	4	0
p.Arg878His	DII S5-P linker	*	0	25904541	5	0	0	0
p.Trp879Arg	DII S5-P linker	0	*	*	2	0	0	0
p.Phe892Ile	DII S5-P linker	0.8	*	*	2	0	0	0
p.Arg893His	DII S5-P linker	*	0	25904541	6	0	3	1
p.Gly897Glu	DII S5-P linker	*	0	25904541	0	1	0	0
p.Glu901Lys	DII S5-P linker	3.2	*	*	6	0	0	0
p.Ser910Leu	DII S6	*	0	24768612	4	0	0	1
p.Leu928Pro	DII S6	1.1	*	*	1	0	0	0
p.Ser1218Ile	DIII S1	*	0	23424222	3	0	0	0
p.Leu1346Pro	DIII S5	1.6	*	*	2	0	0	0
p.Asn1380Lys	DIII S5-P linker	0.2	*	*	2	0	0	0
p.Ser1382Ile	DIII S5-P linker	3.5	*	*	3	0	5	0
p.Gly1406Arg	DIII S5-P linker	*	7.7	16632547	4	0	1	0
p.Gly1408Arg	DIII S5-P linker	*	0	14523039	8	1	19	0
p.Gly1420Arg	DIII S5-P linker	3	*	*	3	0	0	0
p.Gly1420Val	DIII S5-P linker	0	*	*	2	0	0	0
p.Ala1428Val	DIII S5-P linker	0.3	*	*	4	0	2	0
p.Asp1430Asn	DIII S5-P linker	*	0	23612926	2	0	0	0
p.Arg1432Gly	DIII S5-P linker	2.2	0	10727653	1	0	0	0
p.Ile1660Val	DIV S5	*	1.5	17075016	5	2	2	0
p.Gly1661Arg	DIV S5	5.4	*	*	7	0	0	0
p.Ser1672Tyr	DIV S5	0.9	*	*	3	0	0	0
p.Gly1712Cys	DIV Pore Helix	*	0	28219873	1	0	0	0
p.Gly1740Arg	DIV P-S6 Loop	*	0	15057319	2	0	0	0
p.Gly1743Glu	DIV P-S6 Loop	*	0	16945804	10	0	0	0
p.Gly1743Arg	DIV P-S6 Loop	*	0	15023552	12	0	6	0

File S1. Summary of patch clamp data for each variant (.csv)

For each variant, peak current density (normalized to wild-type), voltage of ½ activation, inactivation time, voltage of ½ inactivation, recovery from inactivation, and late current (% of peak) are presented. Means, standard errors of the mean, and the number of qualifying cells are presented for each parameter. Some parameters have "normalized" values also included which indicates the difference in the parameter value from wild-type. Only variants with at least 5 qualifying cells are included, so most severe loss of function variants are not included for most parameters. In addition, variants are classified into categories based on their functional properties, and each variant's BS3 and PS3 ACMG criteria for Brugada Syndrome (loss of function) or Long QT syndrome (gain of function) is presented.

Supplemental Methods

Peak current averaging

For each variant, mean peak current density was calculated as *peak current/capacitance*, averaged across all in voltage control cells. For variants with near-wild-type peak currents, the percentage of cells with detectable currents matched the expected percentage from flow cytometry (Figure 1A-B). However, severe loss of function variants had a substantially lower proportion of wells with detectable currents compared to the predicted percentage from flow cytometry, as is typically observed.[6] Since a simple mean would overestimate the true peak current, an adjustment was made to the means based on a comparison between the flow cytometry and patch clamp data. If the percentage of current-positive wells was >10% less than the expected percentage from flow cytometry, the number of expected additional cells with no current was calculated as follows:

*Expected additional cells = #QC+ cells *(%mCherry+ cells - %QC+ cells with current)*

QC+ cells are defined as cells with a 0.5- 10 GΩ seal resistance and 5-30 pF capacitance. These expected additional cells were added to the peak current density average. For each variant, peak current density averages were first normalized to wild-type cells from the same experiment/transfection, then averaged across independent experiments/transfections.

Building a homology model

Two starting partial models of SCN5A bound with SCN1B, which only covered aligned residues, were generated by threading the sequences of SCN5A and SCN1B onto the two template structures respectively. The threading was guided by the corresponding sequence alignments. Full models were created by hybridization of the two starting models using the

Rosetta comparative modeling (RosettaCM) protocol[7] guided by the RosettaMembrane energy function.[8] The starting model generated from the primary template was used as the base model during hybridization. The boundaries of membrane-spanning segments were calculated using the PPM server[9] based on the starting model generated from the primary template. The boundaries were used to impose membrane-specific Rosetta energy terms on residues within the theoretical membrane bilayer. Fragments in the starting model where coordinates were missing were modeled *de novo* by inserting fragments selected from the Protein Data Bank using local sequence information.[10] Amino acid rotamer conformations were optimized by a nondeterministic Monte Carlo simulated annealing protocol, referred to as rotamer repacking in Rosetta, and models were refined in internal and Cartesian coordinate space by gradient-based minimization. A total of 6000 full models of SCN5A bound with SCN1B were generated using RosettaCM and models ranked by Rosetta energy function in the top 20% were grouped into ten clusters based on pairwise root-mean-square distances. The lowest-energy model from the largest cluster was selected as the final model (Figure 5, S5) for structure-based analysis in this work. This model was also the lowest-energy model across all models sampled.

ΔΔG Calculations

The Rosetta ΔΔG protocol samples conformational degrees of freedom in a locally restricted region around the residue of interest: all sidechains within 6 Å of the mutated residue, and the backbone of a three-residue window around the mutated residue were allowed to move.[11] The sampling was guided by an energy function fitted to recapitulate experimentally determined membrane protein ΔΔG values (Table S6).[12] ΔΔG values computed through this energy function were previously demonstrated to be strongly correlated with cell surface expression levels of human rhodopsin variants.[13] Previous studies have shown that the

magnitude of variant-caused perturbation to protein native thermostability (i.e. $|\Delta\Delta G|$) correlates best with disease likelihood.[14] Accordingly, in this work, variant-induced perturbation to native thermostability ($|\Delta\Delta G_{wild\text{-}type\text{->}variant}|$) was computed as the absolute energy difference between the refined variant structure and the refined wild-type structure: $|\Delta\Delta G_{wild\text{-}type\text{->}variant}| = |\Delta G_{variant} - \Delta G_{wild\text{-}type}|$. Due to the nondeterministic nature of conformation sampling in Rosetta, the $|\Delta\Delta G|$ of each variant was computed 30 times and the average was recorded. The Rosetta energy function is a hybrid of both physically meaningful terms and statistics-based terms, and it does not compute the entropic contribution to the Gibbs free energy in a thermodynamically rigorous manner.[15] Thus, it is best to interpret $\Delta\Delta G$ values computed through the Rosetta energy function in a statistical manner as approximations to the Gibbs free energies.

Literature Cited

1. Richards, S., Aziz, N., Bale, S., Bick, D., Das, S., Gastier-Foster, J., Grody, W.W., Hegde, M., Lyon, E., Spector, E., et al. (2015). Standards and guidelines for the interpretation of sequence variants: a joint consensus recommendation of the American College of Medical Genetics and Genomics and the Association for Molecular Pathology. Genet Med 17, 405-424.
2. Potet, F., Mabo, P., Le Coq, G., Probst, V., Schott, J.J., Airaud, F., Guihard, G., Daubert, J.C., Escande, D., and Le Marec, H. (2003). Novel brugada SCN5A mutation leading to ST segment elevation in the inferior or the right precordial leads. J Cardiovasc Electrophysiol 14, 200-203.
3. Benson, D.W., Wang, D.W., Dyment, M., Knilans, T.K., Fish, F.A., Strieper, M.J., Rhodes, T.H., and George, A.L., Jr. (2003). Congenital sick sinus syndrome caused by recessive mutations in the cardiac sodium channel gene (SCN5A). J Clin Invest 112, 1019-1028.
4. Kroncke, B.M., Glazer, A.M., Smith, D.K., Blume, J.D., and Roden, D.M. (2018). SCN5A (NaV1.5) Variant Functional Perturbation and Clinical Presentation: Variants of a Certain Significance. Circ Genom Precis Med 11, e002095.
5. Kroncke, B.M.S., D.; Glazer, A.; Roden, D.; Blume, J. (2019). A Bayesian method using sparse data to estimate penetrance of disease-associated genetic variants. bioRxiv: https://wwwbiorxivorg/content/101101/571158v1.
6. Pfahnl, A.E., Viswanathan, P.C., Weiss, R., Shang, L.L., Sanyal, S., Shusterman, V., Kornblit, C., London, B., and Dudley, S.C., Jr. (2007). A sodium channel pore mutation causing Brugada syndrome. Heart Rhythm 4, 46-53.
7. Song, Y., DiMaio, F., Wang, R.Y., Kim, D., Miles, C., Brunette, T., Thompson, J., and Baker, D. (2013). High-resolution comparative modeling with RosettaCM. Structure 21, 1735-1742.
8. Barth, P., Wallner, B., and Baker, D. (2009). Prediction of membrane protein structures with complex topologies using limited constraints. Proc Natl Acad Sci U S A 106, 1409-1414.
9. Lomize, M.A., Pogozheva, I.D., Joo, H., Mosberg, H.I., and Lomize, A.L. (2012). OPM database and PPM web server: resources for positioning of proteins in membranes. Nucleic Acids Research 40, D370-D376.
10. Simons, K.T., Kooperberg, C., Huang, E., and Baker, D. (1997). Assembly of protein tertiary structures from fragments with similar local sequences using simulated annealing and Bayesian scoring functions. J Mol Biol 268, 209-225.
11. Park, H., Bradley, P., Greisen, P., Liu, Y., Mulligan, V.K., Kim, D.E., Baker, D., and DiMaio, F. (2016). Simultaneous Optimization of Biomolecular Energy Functions on Features from Small Molecules and Macromolecules. Journal of Chemical Theory and Computation 12, 6201-6212.
12. Kroncke, B.M., Duran, A.M., Mendenhall, J.L., Meiler, J., Blume, J.D., and Sanders, C.R. (2016). Documentation of an Imperative To Improve Methods for Predicting Membrane Protein Stability. Biochemistry 55, 5002-5009.
13. Roushar, F.J., Gruenhagen, T.C., Penn, W.D., Li, B., Meiler, J., Jastrzebska, B., and Schlebach, J.P. (2019). Contribution of Cotranslational Folding Defects to Membrane Protein Homeostasis. J Am Chem Soc 141, 204-215.

14. Casadio, R., Vassura, M., Tiwari, S., Fariselli, P., and Luigi Martelli, P. (2011). Correlating disease-related mutations to their effect on protein stability: a large-scale analysis of the human proteome. Hum Mutat 32, 1161-1170.
15. Alford, R.F., Leaver-Fay, A., Jeliazkov, J.R., O'Meara, M.J., DiMaio, F.P., Park, H., Shapovalov, M.V., Renfrew, P.D., Mulligan, V.K., Kappel, K., et al. (2017). The Rosetta All-Atom Energy Function for Macromolecular Modeling and Design. J Chem Theory Comput 13, 3031-3048.